# American Society of Mechanical Engineers

# GT2020-16280

# OPTIMAL CONTROL OF A COMPOUND ROTORCRAFT FOR ENGINE PERFORMANCE ENHANCEMENT

**Calum Scullion, Stavros Vouros, Ioannis Goulos, Devaiah Nalianda, Vassilios Pachidis**
Cranfield University, Bedford, UK

## ABSTRACT

*Demands for rotorcraft with increased flight speed, improved operational performance and reduced environmental impact have led to a drive in research and development of alternative concepts. Compound rotorcraft overcome the flight speed limitations of conventional helicopters with additional lifting and propulsive components. Further to operational benefits, these augmentations provide additional flight control parameters, resulting in control redundancy. This work aims to investigate the impact of optimal control strategies for a generic coaxial compound rotorcraft, equipped with turboshaft engines, targeting the minimization of mission fuel burn and gaseous emissions. The direct redundant controls considered are: (a) main rotor speed, (b) propeller speed, and (c), fuselage pitch attitude. A simulation tool for coaxial compound rotorcraft analysis has been developed and coupled to a zero-dimensional engine performance model and a stirred-reactor combustor model. Firstly, experimental and flight test data were used to provide extensive validation of the developed models. A parametric analysis was then carried out to gain insight into the effect of the redundant controls. This was followed by the derivation of a generalized set of optimal redundant control allocations using a surrogate-assisted genetic algorithm. Application of the optimal redundant control allocations during realistic operational scenarios has demonstrated reductions in fuel burn and $NO_X$ of up to 6.93% and 8.74% respectively. The developed method constitutes a rigorous approach to guide the design of control systems for future advanced rotorcraft.*

Keywords: compound rotorcraft, coaxial rotor, redundant controls, optimization, gas turbines, environmental impact, aerodynamics, control, aerospace, design.

## NOMENCLATURE
**Acronyms**

| | |
|---|---|
| $CO_2$ | Carbon dioxide |
| DSE | Design space exploration |
| EMS | Emergency medical services |
| FADEC | Full authority digital engine control system |
| FPT | Free power turbine |
| LOOCV | Leave-one-out-cross-validation |
| MCP | Maximum continuous power |
| MTOW | Maximum take-off weight |
| $NO_X$ | Nitrogen oxides |
| PAT | Passenger transport |
| SAR | Search and rescue |
| VPS | Variable propeller speed |
| VRS | Variable rotor speed |

**Symbols**

| | |
|---|---|
| h | Density altitude [m] |
| k | Fuselage drag factor [m$^2$] |
| $\dot{m}_f$ | Fuel flow rate [kg/s] |
| $\Delta\dot{m}_f$ | Fuel flow delta [%] $= 100\,(\dot{m}_f - \dot{m}_f^{Nom})/\dot{m}_f^{Nom}$ |
| V | Flight speed [m/s] |
| W | Rotorcraft gross weight [kg] |
| $\Omega$ | Rotational speed [rad/s] |
| $\overline{\Omega}$ | Rotational speed ratio [%] $= 100\,(\Omega\,/\,\Omega^{Nom})$ |
| $\theta_f$ | Fuselage attitude (positive nose-up) [deg] |

**Sub/superscripts**

| | |
|---|---|
| MR | Main rotor |
| Nom | Nominal |
| Opt | Optimal |
| P | Propeller |

## 1 INTRODUCTION
### 1.1 Background

There is an increasing demand for rotorcraft with improved operational performance and reduced environmental impact. Compound rotorcraft have emerged as one promising concept to meet these challenging requirements. Many different configurations are currently being explored in academia and industry as a result of the large design space opened up by the addition of supplementary lifting and propulsive components. One of the most notable compound architectures is Sikorsky's X2 technology [1, 2]. This differs significantly from conventional helicopters, employing a stiff counter-rotating coaxial rotor system, a pusher propeller and turboshaft engines. A demonstrator has already proven the technology, while scaled up versions are currently in development [3].

For coaxial rotorcraft, the addition of the propeller, second rotor, empennage control surfaces, and main rotors-engine speed control results in up to 10 direct pilot controls [4–6]. Conventional helicopters typically employ only four direct controls, with fuselage roll and pitch attitude being uniquely determined through application of the six degrees of freedom equilibrium equations [7]. The coaxial rotorcraft additional pilot controls, therefore, result in control redundancy, as the number of controls exceeds the degrees of freedom. This control redundancy allows the aircraft to be trimmed in non-unique states for a designated flight condition. This enables the redundant trim controls to be optimized for a given flight state to achieve improved fuel economy and reduced environmental impact.

## 1.2 Compound rotorcraft control redundancy

The best use of compound rotorcraft control redundancy has received significant attention in recent years as the development of compound rotorcraft has accelerated. Reddinger *et al.* [8–10] assessed a compound derivative of the UH-60A helicopter in a high speed cruise state. They examined the influence of rotor speed, propeller thrust, stabilator pitch, and aileron deflection on power and vibration levels. Their main finding was that an optimal power state was attained with a near level fuselage attitude. Jacobellis *et al.* [4] examined the effect of propulsive thrust, differential lateral cyclic, and main rotors speed toward minimization of power and vibrations of the Sikorsky XH-59A coaxial compound rotorcraft in high speed cruise. A three-degree pitch up fuselage attitude and 80% nominal main rotors speed was optimal for minimizing power at 230 kts.

Herrmann *et al.* [5,6] conducted a multi-objective optimization to minimize a combination of power, fatigue, and noise. An 18-tonne generic coaxial rotorcraft derived from scaling up the Sikorsky X2 was used. The impact of varied fuselage attitude and horizontal stabilizer elevator were assessed between 160 and 250 kts. Their studies suggested that a positive fuselage attitude was optimal for minimizing power. This resulted from the main rotors propulsive thrust requirement being removed, and a component of the free-stream acting as upwash through the rotor. They also demonstrated that a further increase in attitude was beneficial for noise levels, as the main rotors were offloaded, and blade-vortex interactions reduced.

The concept of variable rotor speed (VRS) has been explored for helicopters and included in several compound rotorcraft control redundancy studies [4,8–10]. Typically, a fixed gearing ratio is employed between the free power turbine (FPT) and main rotor. Therefore, the engine's full authority digital engine control system (FADEC) is used to alter the FPT speed and hence rotor speed. Conventionally, the FADEC continuously alters the fuel flow rate to maintain a constant FPT and thus rotor speed. As a result, the benefits that VRS can provide from an aerodynamic perspective must be considered alongside the engine performance implications. The coupled response has been investigated for single main and tail rotor configurations [11–14], but not for compound rotorcraft.

Misté *et al.* [11–13] investigated the effect of VRS for a UH-60A helicopter, including both the aerodynamic and engine thermodynamic effects. They demonstrated engine fuel flow reductions of 7-8%. These improvements were restricted to near endurance flight speed and low gross weight and/or altitude conditions. Goulos and Bonesso [14] extended the scope of VRS

assessments to mission level for a Bo 105 helicopter. For the full operational envelope, schedules of optimal VRS and active blade twist that minimize fuel flow were derived. The fuel burn and $CO_2$ reductions by utilizing these at mission level ranged from 0.5% for a passenger transport mission (PAT), rising to 5% for a search and rescue (SAR) mission. This highlights the need to assess these types of technology at mission level, for realistic operating scenarios. The mission level improvements are strongly dependent on the proximity and time spent in operating states where these technologies are beneficial.

VRS has a further implication for helicopter performance as the tail-rotor employs a fixed transmission ratio to the main rotor and FPT. Han and Barakos [15] investigated the effect of a tail rotor with independently variable speed. For the UH-60A helicopter, they demonstrated that this could provide up to a 1% power reduction relative to the fixed gearing ratio case. The impact of a fixed gearing ratio may also be significant for compound rotorcraft, where a propulsive propeller replaces the tail-rotor. Although the role and operation of the propeller differ, there will be an impact from varying its rotational speed. Therefore, using VRS to search for rotorcraft performance enhancement must also incorporate the implications of altering the propeller speed. As a result, investigating a fixed gearing ratio propeller relative to independently variable propeller speed (VPS) is of interest. At this preliminary level, utilizing a continuously variable system is acceptable, as it will inform the discrete ratios of interest. This topic is currently being addressed by Sikorsky [16], who are researching concepts for multi-speed tail-rotor or propeller gearboxes. Any benefit that can be obtained, however, will have to be considered against the detriment in performance arising from the additional weight of a multi-speed gearbox, or similar system.

## 1.3 Scope of present work

Existing assessments of compound rotorcraft control redundancy have been limited to consideration of power, vibration, and noise at idealized trim points [4–6,8–10]. No previous work has included the coupled response of variable main rotors-engine-propeller speed, or the optimization of redundant controls at mission level towards fuel burn and environmental impact reduction. Additionally, no examination of the effectiveness of VPS has been undertaken.

This work aims to investigate optimal redundant control allocation for a coaxial compound rotorcraft toward engine performance enhancement at mission level. The investigated aircraft architecture is modeled after a generic twin-engine medium coaxial rotorcraft. A simulation methodology for coaxial rotorcraft trim analysis, mission simulation, engine performance [17], and emissions prediction [18] is developed and validated for each respective discipline. An approach for allocating the optimal redundant controls at mission level is deployed, which consists of design space exploration (DSE) and global optimization [14]. The developed simulation framework is used to investigate the impact of the direct redundant controls, VRS and VPS, in addition to the resolved redundant control, fuselage attitude. The DSE and global optimization approach facilitates extension of the analysis to mission level. This work contributes to the existing literature by providing insight into best practices for optimal redundant control allocation for future civilian rotorcraft.

## 2  METHODOLOGY

An integrated methodology has been developed for simulation of coaxial compound rotorcraft. Models for rotorcraft performance and mission analysis were developed and coupled to software for engine performance and gaseous emissions prediction, enabling analysis of the coupled airframe-engine performance. The framework is extended with an approach to enable optimal redundant control allocation at mission level. This employs models for design space exploration, surrogate modeling, and global optimization.

### 2.1  Coaxial rotorcraft performance

The performance model has been developed to approximate Level 1 of Padfield's modeling hierarchy and is therefore appropriate for performance studies [7]. The main rotor model uses steady-state non-linear blade element theory, with the inflow modeled using Beddoes model, as extended by van der Wall [19]. In low-speed flight, the interference between the two rotors is estimated using an empirical model derived in Ref. [20]. This model was developed for hover, but an extension of this based upon the assumption that the interaction reduces with the wake skew angle is adopted [21,22]. The blades are assumed rigid, with flap deflections accounted for using Padfield's analytical method [7]. This requires the equivalent spring stiffness for the first harmonic of blade flapping, which is set to 1.4, as determined for the Sikorsky X2TD blades [1].

The propeller model utilizes steady-state non-linear blade element momentum theory (BEMT) [23]. The empennage is represented using look-up tables for lift and drag coefficients as a function of angle of attack, employing experimental data for the Bell XV-15 horizontal and vertical stabilizers [24]. The empennage of this tilt-rotor is of the same design as the coaxial compound rotorcraft, and hence this data provides an appropriate representation. The fins are considered to be all moving surfaces and provide yaw control above a moderate flight speed.

Due to the lack of data available for the aerodynamic characteristics of the compound rotorcraft streamlined fuselage, aerodynamic coefficients as a function of angle of attack are based upon Bell XV-15 isolated fuselage testing [24]. Although this is a tilt-rotor aircraft, inspection of the fuselage geometry shows that this is more representative of a streamlined compound fuselage than a conventional helicopter. The zero-incidence flat plate drag area is defined by the empirical relation proposed by Harris [25]; $k(MTOW[kg] / 454[kg])^{2/3}$. The fuselage drag factor, $k$, accounts for the fuselage type and technology factors. The value of $k$ may be selected based on literature suggestions for current low-drag designs, 0.232 m$^2$ [25] or optimistic conceptual design studies, 0.149 m$^2$ [26,27]. An empirical basis is used to determine the rotor hub drags, which utilizes a drag coefficient based on the rotor disc area. A drag coefficient of 0.0024 is representative of current low-drag designs, while 0.0015 represents faired hubs with active flow control [27]. The total airframe drag is therefore constituted of components from the fuselage, both rotor hubs, inter-rotor shaft, and empennage.

For any specified operating condition and control inputs, the force and moments of each component are determined and resolved to the aircraft's center of gravity. A Newton-Raphson root finding algorithm is applied to determine the controls required to attain an equilibrium state in the six free flight degrees of freedom. An additional trim target is included which prescribes the lift-offset of the coaxial rotor system, as frequently employed for coaxial rotor modeling [6,28]. This enables the model to be configured for various rotorcraft setups. Lift-offset defines the lateral distance from the rotor's center of rotation to center of lift [29]. Due to the stiff coaxial rotor design, each rotor can operate with increased efficiency by generating more lift on the advancing side of the rotor disk than the retreating [29].

### 2.2  Gas turbine performance (TURBOMATCH)

TURBOMATCH is incorporated within the framework to estimate fuel flow and provide combustor inlet conditions for gaseous emission prediction. TURBOMATCH utilizes zero-dimensional aero-thermal analysis, and is capable of point or transient analysis, at design or off-design conditions. Model development and validation of rotorcraft turboshaft engines were carried out by Goulos *et al.* [30] and Ortiz-Carretero *et al.* [31].

### 2.3  Gaseous emissions prediction (HEPHAESTUS)

HEPHAESTUS is a gaseous emission prediction software developed for civil aero-engines [32] and extended for turboshaft engines [33]. The model is based on the stirred reactor concept, combined with simplified chemical reaction equations. The specific combustor geometry is accounted for and must be defined in terms of primary, intermediate, and dilution zone volumes, in addition to the air mass-flow fractions. The emission indices may be calculated for any given operating and combustor inlet conditions. Extensive validation for the emission indices prediction for turboshaft engines has been conducted by Ortiz-Carretero *et al.* [31] and Goulos *et al.* [33].

### 2.4  Mission analysis

The mission analysis procedure is based on that reported by Goulos *et al.* [34], adapted for compound rotorcraft missions. The current integration of the models within the mission simulation framework is illustrated in Fig. 1. For the flight path model, a Cartesian reference frame is used. Inputs are provided as modular blocks; idle, payload, hover, cruise, and loiter, which can be placed together to define any mission type. The transient regions are ignored, with the rotorcraft assumed to operate in a steady trimmed condition during each discretized mission segment. The rotorcraft trim point analysis is conducted for each segment in turn, with the operating conditions provided by the flight path model. The rotorcraft gross weight is updated for the fuel burned following each segment and for any change in the payload. As a result of the continuously varying flight conditions and potentially payload change during a mission, determination of the required mission fuel is not trivial, therefore, a fixed-point iterative numerical method is used to converge on this [34].

### 2.5  Design space exploration, surrogate modeling and optimization

Mission level assessment requires a mechanism to determine the optimal redundant controls at every operating point encountered during any given mission. Goulos and Bonesso [14] introduced an approach to derive optimum schedules of rotor speed and active blade twist throughout the operational envelope of a helicopter. They employed DSE, modeling and global optimization. The operating conditions were included in the design space alongside the redundant controls. This enabled the optimal redundant controls to be determined for any specified operating point. Employing surrogate models rather than direct non-linear simulation

3
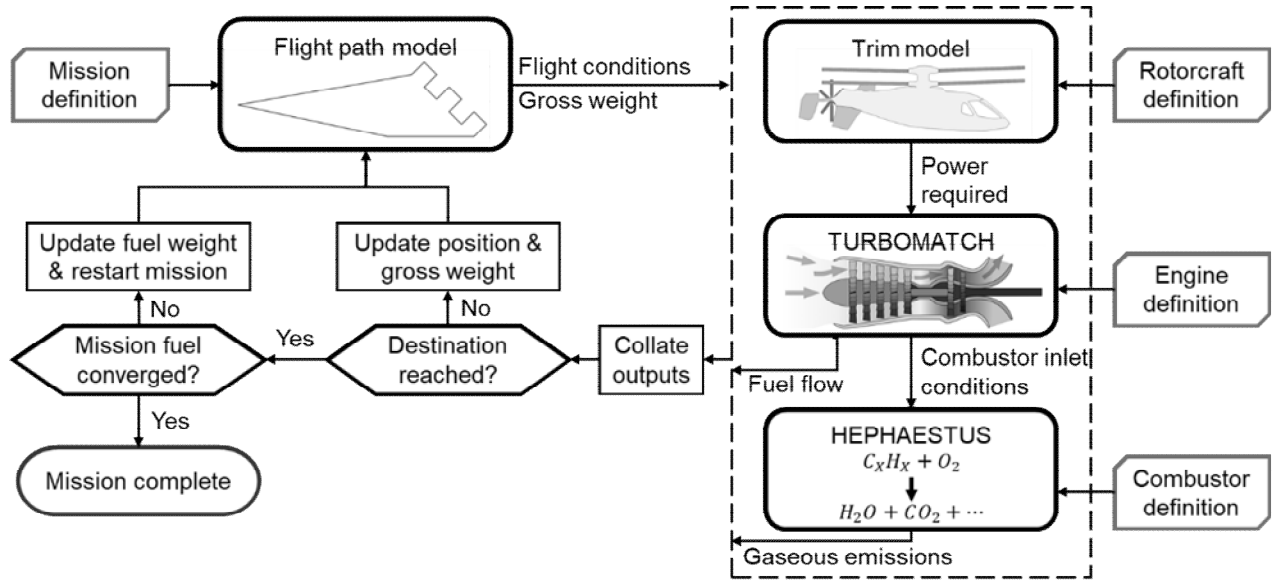
**Figure 1:** Mission analysis framework flowchart

reduced the optimization task to practical computational time. Consequently, this method enables allocation of the optimal redundant controls at any operating condition, in an efficient manner, and therefore, mission level assessments can be conducted.
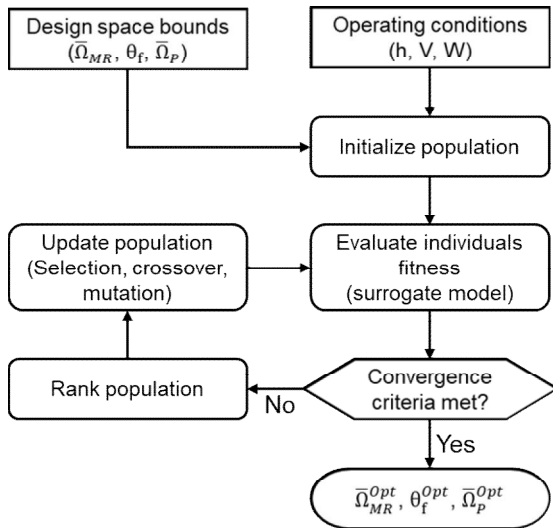


**Figure 2:** Synthesis of mission analysis and global optimization for control allocation

This method consists of three tasks. The first is a design of experiments, the purpose of which is to extract the maximum amount of information from the design space, from the minimum number of samples. The Latin hypercube design (LHD) algorithm was selected, having been shown as an efficient method for this purpose [35]**.** Once the samples have been defined, a trim point analysis is conducted for each, returning the fuel flow and gaseous emissions rates. Surrogate models may then be derived from the samples using Kriging interpolation [36]. The accuracy of the surrogate models was assessed using leave-one-out-cross-validation (LOOCV) [37]. The derived surrogate models were able to evaluate the fuel flow or gaseous emissions at any operating condition and combination of the redundant controls. A global optimization algorithm can, therefore, interrogate the surrogate models for a specified condition to determine the optimal redundant controls. The

global optimization technique selected for this purpose was the non-dominated sorting genetic algorithm II (NSGA-II) [38]. Application of a global optimization algorithm prevents the solution from being trapped in any local optimums across the design space. Further detail on each aspect of this approach has been provided by Goulos and Bonesso [14].

To apply this method to mission level, the simulation framework provides the operating conditions at each waypoint of the mission to the optimization algorithm. The optimization algorithm utilizes the surrogate models to ascertain the optimal redundant controls, thus providing these to the simulation framework. The optimization process and integration with the simulation framework is illustrated in Fig. 2. The adopted approach has been adapted for compound rotorcraft control redundancy studies, enabling multiple redundant controls to be assessed within the newly developed simulation framework.

## 2.6 Reference rotorcraft definition

To enable the objectives of this work to be achieved, a generic coaxial compound rotorcraft was defined. The configuration is modeled after the Sikorsky X2TD [1,2], scaled up to be representative of future civilian compound rotorcraft, with a passenger capacity of 12 [39]. This resulted in a scaling up of the maximum take-off weight (MTOW) by a factor of 2.67. The rotorcraft comprises a streamlined fuselage, a counter-rotating coaxial rotor system, and a six-bladed pusher propeller, as illustrated in Fig. 3. The selected powerplant is modeled after a General Electric T700-GE-700 turboshaft. Table 1 provides the main design parameters.
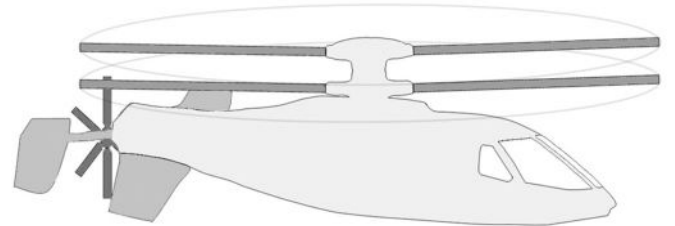


**Figure 3:** Generic coaxial compound rotorcraft configuration

The main rotor geometry is modeled after the Sikorsky X2TD, as described in Ref. [40,41]. Lateral lift-offset is prescribed as a linear trend from zero in hover to 15% of the rotor

4

radius at a flight speed of 100 m/s. This trend approximates the operation of the Sikorsky X2TD from published flight test data [2]. The main rotors speed is reduced in high-speed flight to prevent transonic effects, by limiting the advancing blade tip Mach number to 0.9 [40]. As shown in Table 1, the airframe drag is between current low-drag and optimistic conceptual studies [25–27]. Similarly, the hub drags are between current low-drag designs and faired hubs with active flow control [27].

In line with current compound rotorcraft developments, the pusher propeller is clutched, so that it may be disengaged in low-speed flight [42]. When disengaged the propeller is assumed to auto-rotate, however, any drag generated is neglected as it is considered to be of a low level relative to the rest of the airframe. Above a flight speed of 40 m/s, the propeller is engaged. This follows findings by Yuan *et al.* [43], who demonstrated that for the XH-59A coaxial compound, operating without the propeller below 47 m/s resulted in lower required power. Below this speed, the fuselage attitude is not redundant and becomes a determined trim parameter. Above it, the fuselage attitude is prescribed at a one degree nose-up attitude, to offload the rotors and operate it in a favorable low-power condition [4,5]. The propeller blade pitch is thus a direct trim control. In the nominal case, a fixed gearing ratio couples the main rotors and propeller speed. However, it is assumed that the propeller speed can be varied independently of the main rotors speed, although the weight of this system is not incorporated, therefore, any benefits that are attained will not include these implications.

**Table 1:** Coaxial compound rotorcraft design parameters

| Parameter | Units | Value |
|---|---|---|
| MTOW | kg | 7280 |
| Empty weight | kg | 4774 |
| Fuselage drag factor, k | $m^2$ | 0.18 |
| Hub drag coefficient | - | 0.0018 |
| Main rotors shaft tilt | deg | 0 |
| Main rotors radius | m | 6.5 |
| Main rotors solidity | - | 0.14 |
| Main rotors speed | rad/s | 28.7 |
| Propeller radius | m | 1.75 |
| Propeller solidity | - | 0.17 |
| Propeller speed | rad/s | 165 |
| Engine | - | T700-GE-700 |
| Engine number | - | 2 |

## 3 RESULTS AND DISCUSSION
### 3.1 Comparison with experimental data
Validation of the rotorcraft performance model was conducted by assessing a flight speed sweep of the Sikorsky X2TD. These simulations were conducted by assuming the propeller provided no thrust below 30 m/s. Above this speed, the fuselage attitude ($\theta_f$) was prescribed, with a linear increase from $\theta_f = 0$ deg. to 2 deg. between 30 and 60 m/s. Thereafter, $\theta_f = 2$ deg. was maintained. This trend was selected following flight test observations by Walsh *et al.* [2], stating that $\theta_f$ ranged from 2 – 5 deg. The main rotors speed was maintained at the nominal, except when the advancing tip Mach number would exceed Mach 0.9, in which case this was reduced.

Figure 4 demonstrates a comparison of rotor and propeller power from simulation results with flight test data [2], and CAMRAD II simulation [44]. Following the procedure of Johnson *et al.* [44], gross weight was maintained at the MTOW for the flight speed sweep. The notable scatter in flight test data

is due to the compilation of this data from a large number of flight tests, normalized to a single altitude in Ref. [2]. The expected trends are shown, with rotor induced power dominant in hover and low-speed flight, while the propeller is feathered to produce negligible propulsive force. It is observed that the power of the main rotors decreases toward a near auto-rotating state above 60 m/s. In this condition, the propeller is used to overcome the airframe parasitic drag, in addition to the rotor drag, while the rotor must only provide a lifting force to balance the weight. Overall, a very good agreement between the flight test data and simulation is shown for both the rotor and propeller power. The root-mean-square (RMS) error relative to the flight test data, normalized by total power (rotors plus propeller), is estimated at 7.27 and 2.38% for the main rotors and propeller power respectively. Furthermore, similar results are observed between CAMRAD II and the present simulations. Between 50 and 100 m/s, the summative power of the main rotors is slightly higher and propeller power lower than CAMRAD II. This indicates that a slightly higher fuselage attitude was used for CAMRAD II simulations, as this would reduce main rotors power, but increase the propulsive thrust required.
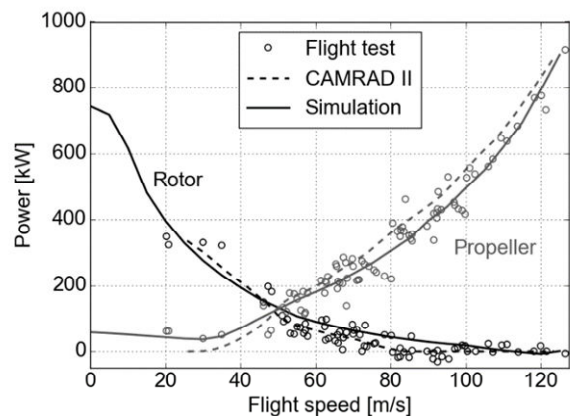


**Figure 4:** Trim results for the Sikorsky X2TD – comparison with flight test data [2] and CAMRAD II simulation [44] for main rotors and propeller power at an altitude of 1219 m

The isolated BEMT propeller model was validated with test data of propeller III from Ref. [45]. Propeller III is a straight bladed, 1.524 m radius, two bladed propeller. It has a design advance ratio of 2, and was intended for investigation over a wide range of blade loading and helical tip Mach numbers [45]. The blades use NACA-16 series airfoils, for which aerodynamic coefficient maps, from an experimental campaign, are available from Ref. [46]. This aerodynamic data encompasses Mach numbers from 0.3 up to 0.9, with Reynolds numbers representative of the propellers root chord. The key concern in this study is the efficiency of the propeller for a wide range of operating conditions. Therefore, for each experimental data point the blade pitch was trimmed to provide the experimental thrust coefficient, with the resulting power coefficient ($C_P = P / (\rho A (\Omega R)^3)$) shown in Fig. 5. A good agreement is illustrated, with an overall $C_P$ RMS error of 6.76%. The majority of the deviation may be attributed to the low advance ratio high loading cases, where a large portion of the blade span experiences stall. Poor prediction in this region is typical of the level of modeling fidelity employed [47], as a result of limitations in the 2D airfoil section aerodynamic data post stall. However, these conditions will not typically occur over the range of operational conditions of interest for a tail-mounted pusher propeller.

5
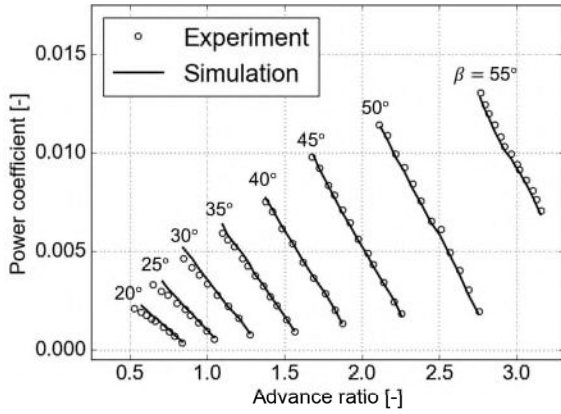
**Figure 5:** Propeller power coefficient prediction of propeller III from Ref. [45] at 1350 RPM, blade pitch annotated – comparison with wind tunnel data from Ref. [45]

Fuel flow rate with gas generator speed and shaft power for a TURBOMATCH T700-GE-700 model are shown in Fig. 6, with simulation data extracted from Refs. [48,49]. A good match is shown between all simulation models. The T700-GE-700 model setup and detailed validation were provided by Ortiz-Carretero *et al.* [31], in addition to setup and extensive validation of a HEPHAESTUS T700-GE-700 model, thus further detail will be omitted.
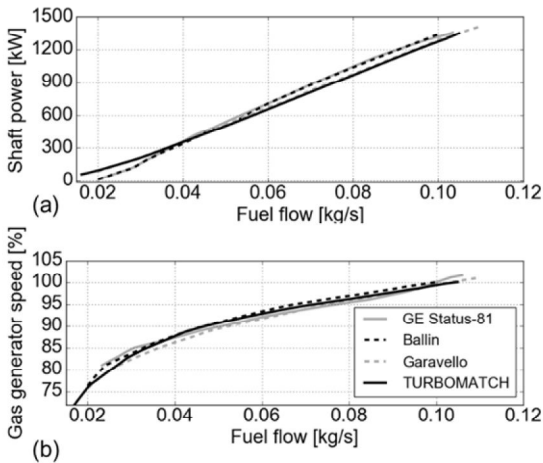


**Figure 6:** Simulation results for the T700-GE-700 – comparison with various simulation models [48,49]: Fuel flow versus (a) shaft power and (b) gas generator speed

## 3.2 Design space behavior

Having developed a simulation model capable of assessing the coaxial compound rotorcraft in terms of airframe and engine performance, parametric studies were undertaken to ascertain the impact of the redundant controls.

Helicopters require the main rotor to provide both the lifting and propulsive force and therefore pitch increasingly nose-down with flight speed to counteract rising drag. The compounds propeller enables the main rotors propulsive requirements to be relieved, and thus the fuselage is no longer required to pitch down. For the generic coaxial rotorcraft, the primary effect of varying the fuselage attitude is to alter the split in overall propulsive force between the main rotor system and the pusher propeller. At a positive attitude, nose-up, the rotors contribute significantly to the overall drag. They also operate with low power demand due to a component of the free-stream acting as an upwash, and the requirement to provide propulsive force

being eliminated. As $\theta_f$ is decreased, the main rotor system thrust vector is tilted forward and hence its net drag tends to reduce until it starts contributing a net propulsive force. As a result, the required propeller thrust will reduce as $\theta_f$ decreases.

Figure 7 illustrates the effect of fuselage attitude on fuel flow relative to the nominal case, $\theta_f^{Nom} = 1$ deg. This nominal fuselage attitude was selected based on the literature review, indicating that a slightly nose-up $\theta_f$ is optimal [4,5]. $\theta_f^{Opt}$ reaches a minimum for flight speeds (V) < 60 m/s, where it is found to be optimal to operate with the main rotors providing the majority of the propulsive force. At V < 60 m/s, the airframe drag is low, therefore the propulsive force required is low, and the propeller operates inefficiently as it is far from its cruising flight design point. As a result, tilting the rotor system thrust vector forward efficiently produces the required propulsive force. $\theta_f^{Opt}$ increases to near −1 deg. for V > 80 m/s. In these conditions, the main rotors are still contributing a small net drag force, however, this is reduced compared to the higher attitude cases. Consequently, the required propeller thrust is reduced, and hence it is found to operate more efficiently. Considering an example at V = 90 m/s with the attitude being decreased from $\theta_f = 1$ to -1 deg. The rotors net drag reduces by 81%, the rotors power doubles, and the propeller propulsive efficiency increases from 81.3% to 83.9%. Overall, this results in a 6.5% power saving relative to the nominal case in this condition. For every gross weight and operating condition, there is a different optimum fuselage attitude, which is governed by the trade-off between rotor and propeller performance.
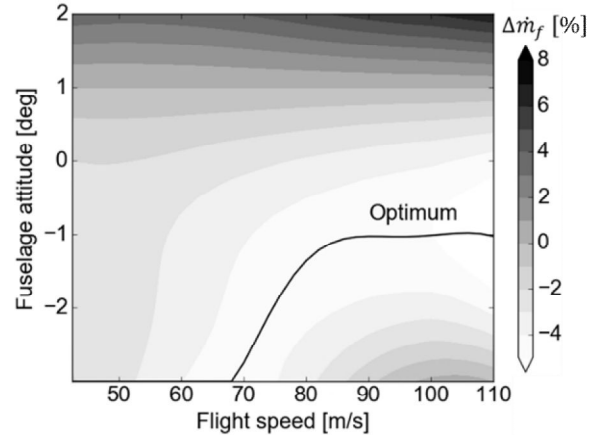


**Figure 7:** Impact of fuselage attitude on trim analysis fuel flow relative to the nominal rotorcraft, W = 7000 kg, h = 1000 m

The impact of VRS ($\overline{\Omega}_{MR} = 100(\Omega_{MR}/\Omega_{MR}^{Nom})$) with flight speed and gross weight (W) is shown in Fig. 8. For V < 40 m/s, the propeller is disengaged, and hence the behavior observed with rotor speed variation comprises the coupled main rotors-engine response. For V > 40 m/s, the propeller is engaged, and the propeller speed is considered to operate with a fixed gearing ratio to the main rotors, hence rotor speed variations will also impact the propeller performance. The hashed regions in Fig. 8 indicate conditions in which a trim state was not achievable due to the rotor and/or propeller being unable to generate enough thrust to maintain a steady flight state. A line of optimum main rotors speed is annotated on each of the figures, indicating that there is a distinct optimum speed for each operating condition.

Goulos and Bonesso [14] have previously provided analysis on the mechanisms governing VRS for a helicopter, elaborating

6

on the coupled main rotor and engine thermodynamic implications. For the coaxial compound rotorcraft, three different aspects govern the behavior observed in Fig. 8: main rotor aerodynamics, engine performance, and propeller aerodynamics. Considering the aspect of rotor aerodynamics, reducing the rotor speed results in a reduction in local blade velocity, and therefore can reduce the profile power. This also reduces the lift generated by the blades, consequently, an increase in blade collective is required to maintain thrust. In conditions where the rotor blades are lightly loaded, and thus have a large stall margin, the benefits of this may be substantial. If the blade loading is high, and hence the stall margin is low, then raising the collective may reduce the airfoil section performance or even result in stall. The rotor aerodynamic considerations, therefore, target maintaining the blade sections at an optimal lift to drag ratio. In high-speed flight, it may also be beneficial to reduce the rotor speed to minimize transonic flow on the advancing blade tips and the associated drag rise.
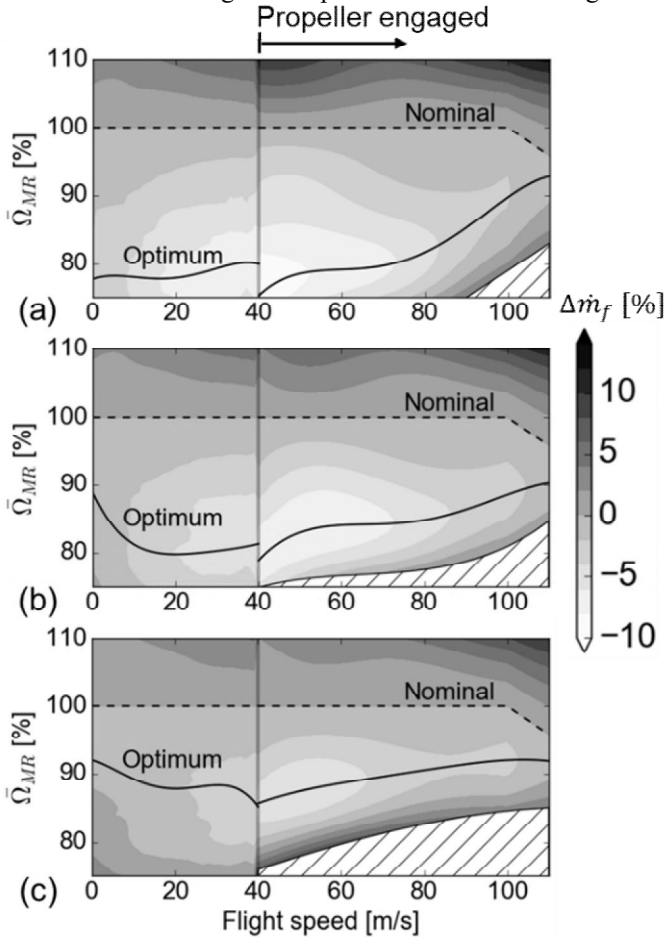


**Figure 8:** Impact of VRS ($\bar{\Omega}_{MR}$) and flight speed on fuel flow relative to the nominal rotorcraft at h = 1000 m: (a) W = 5000 kg, (b) W = 6000 kg, and (c) W = 7000 kg

The impact of rotor aerodynamics explains the trends observed with increasing gross weight in Fig. 8. The blade loading increases with weight, therefore the optimal main rotors speed increases. Furthermore, the potential fuel flow benefits are shown to decrease with increasing weight in hover, with a 2.5, 1.2, and 0.4% fuel flow reduction attained. Near endurance flight speed, around V = 45 m/s, the largest fuel flow reductions are reached, $\Delta \dot{m}_f = -10.2$, -7.6, and -5.5%, at $\bar{\Omega}_{MR} = 75$, 80, and 87%, with increasing weight. Reduced $\bar{\Omega}_{MR}$ is most beneficial in

this condition due to the low induced power, high profile power, and relatively low thrust requirements. Potential fuel flow reductions with VRS are shown to diminish with increasing flight speed. However, as discussed in the subsequent section, this may be due to the increasing level of propeller loading with flight speed, and the associated implications of VRS on the propeller aerodynamics.

Isolating the engine performance under variable FPT conditions is necessary to attain a complete understanding of the airframe-rotor system with VRS. Figure 9 illustrates this by simulation of the T700-GE-700 using TURBOMATCH. As shaft power increases, the optimal FPT speed also increases. It is also noted that the maximum continuous power setting (MCP) corresponds to the point where the optimal line crosses 100% FPT. This corresponds to the nominal main rotors speed for a fixed gearing ratio [14]. At power settings less than MCP an FPT speed reduction may be beneficial, and hence this could be complementary to rotor speed reduction. However, in high-speed flight or near hover, where a high power setting is required, the rotor and FPT speed optimums may diverge. In these conditions, the rotor performance may improve from reducing speed, as indicated in Fig. 8, but this may reduce the engine thermodynamic efficiency.
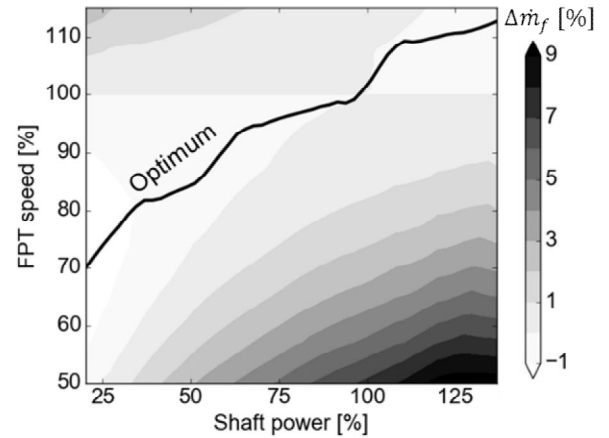


**Figure 9:** Impact of FPT speed with shaft power relative to MCP on fuel flow for the T700-GE-700

The next consideration results from propeller aerodynamic performance. The mechanisms governing the effect of rotational speed are the same as for the rotor, their operation throughout flight, however, differ significantly. The propellers role is to generate propulsive thrust to overcome drag. As flight-speed is increased the total airframe drag will grow, therefore, the propeller blade loading will tend to increase. With the same governing mechanisms as the rotor aerodynamics, a reduced propeller speed may be beneficial at lower flight speed, but with high loading at high-speed, it will likely be detrimental.

Figure 10 shows the impact of altering propeller and rotor speed independently ($\bar{\Omega}_P \neq \bar{\Omega}_{MR}$) for three flight speeds. The nominal point is annotated, along with a line of fixed gearing ratio, which indicates the behavior of the non-VPS system ($\bar{\Omega}_P = \bar{\Omega}_{MR}$). At V = 50 m/s, Fig. 10(a), the coupled main rotors-propeller speed reaches a near optimal state at $\bar{\Omega}_{MR/P} = 83$%, with an 8.5% fuel flow reduction. Decoupling the propeller speed gives just a 0.2% further benefit. At V = 75 m/s, a 5.2% improvement is attainable, which corresponds to $\bar{\Omega}_{MR/P} = 85$%. In the high-speed case, $\bar{\Omega}_{MR/P} = 91$% provides a 2.9% improvement, however, when decoupled this increases to 3.8%.

7
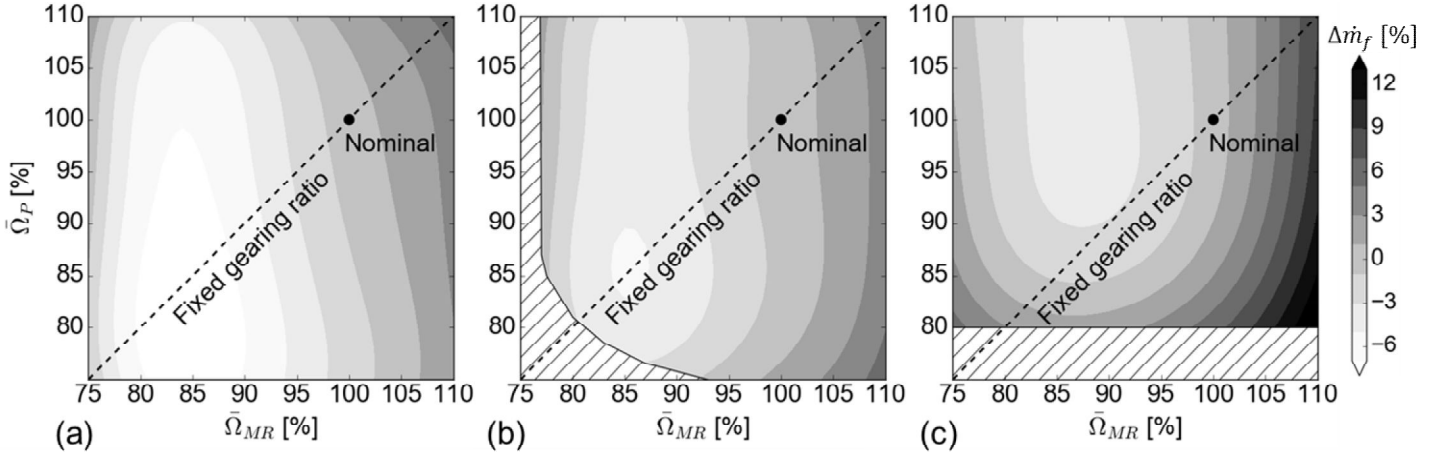
**Figure 10:** Impact of VPS and VRS on fuel flow relative to the nominal rotorcraft for W = 6000 kg, h = 1000m, and V = (a) 50 m/s, (b) 75 m/s, and (c) 100 m/s

The optimum main rotors speed increases slightly with flight speed, shown as a shift in the minimum fuel flow region from left to right in Figs. 10(a)-(c). The optimum propeller speed changes more significantly, increasing from $\bar{\Omega}_P$ = 75% at V = 50 m/s to $\bar{\Omega}_P$ > 100% at V = 100 m/s. Independently optimal main rotors and propeller speeds exist in many conditions; however, there will be a flight speed for every gross weight and altitude where the optimal speeds coalesce. Despite this, the advantage of varying the propeller speed independently of the main rotors in high-speed flight is clear.

The results in this section have shown that there is potential to improve the overall airframe-engine performance through multidisciplinary optimization of the redundant control parameters. For the operating conditions shown, isolated fuselage attitude optimization may provide a fuel flow reduction of up to 4%, while VRS has shown up to a 10% reduction. The implication of decoupling main rotors and propeller speed has been discussed, highlighting a potential fuel flow reduction this operating state up to 0.8%. The next step in the analysis is thus to determine the optimum combination of these redundant controls as a function of operating conditions.

**Table 2:** Design space parameter bounds

| Parameter | Symbol | Units | DSE Bounds 1 | DSE Bounds 2 |
|---|---|---|---|---|
| Gross weight | W | kg | 4800 – 7280 | 4800 – 7280 |
| Flight speed | V | m/s | 0 – 40 | 40 – 115 |
| Altitude | h | m | 0 – 3000 | 0 – 3000 |
| Rotors speed | $\bar{\Omega}_{MR}$ | % | 75 – 115 | 75 – 115 |
| Fuselage attitude | $\theta_f$ | deg | - | -3 – 3 |
| Propeller speed | $\bar{\Omega}_P$ | % | - | 75 – 110 |

### 3.3 Design space exploration and surrogate modeling

The preceding analysis of the design space behavior provided an understanding of the potential benefits of the redundant controls and the mechanisms behind this. Furthermore, it provided insight into bounds that will capture the optimal redundant controls throughout the operational envelope. The bounds selected are shown in Table 2, alongside each design space parameter. The main rotors speed bounds were selected to capture under and over-speed conditions. The fuselage attitude was bounded based on parametric studies to ensure the optimal value will be captured, and the propeller speed upper bound was set to keep the tip Mach number below supersonic conditions.

The operating conditions of gross weight and flight speed are based upon the reference rotorcraft specification and capabilities, whilst the maximum altitude was based on cabin pressurization limits [50].

Due to the propeller being engaged at V = 40 m/s, the design space was separated into two regions. For V < 40 m/s, fuselage attitude and propeller speed are not redundant, therefore the first DSE includes the gross weight, altitude, and main rotors speed, with V = 0-40 m/s. The second consists of V = 40-115 m/s, in addition to fuselage attitude and propeller speed. For the first DSE 1000 samples were used. This number was selected based on previous VRS DSE studies [14]. This was increased to 8000 for the second DSE due to the increase in number of parameters, bounds, and likelihood of the combined redundant controls resulting in a situation where a trim solution was not attainable.
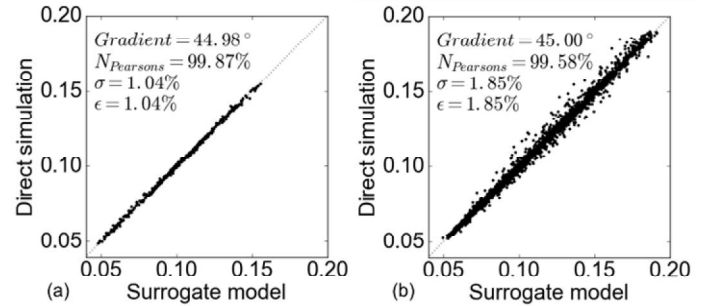


**Figure 11:** Leave-one-out-cross-validation for the fuel flow surrogate models: (a) DSE 1, (b) DSE 2

With the design space defined, the LHD algorithm was deployed to generate sample points. For each sample, a trim point analysis was conducted with the simulation model. The Kriging interpolation method was provided with the resulting data to generate surrogate models of fuel flow and gaseous emissions rates. The derived surrogate models utilized the squared-exponential correlation model, a constant regression model, and a nugget of 0.001. These three options were selected following sensitivity analysis of their impact on LOOCV RMS error. Figure 11 illustrates the LOOCV results for the fuel flow models. The accuracy is quantified with the RMS error, standard deviation, Pearson's correlation coefficient, and a line of best-fit gradient through the predicted versus direct results. RMS errors of 1.04% and 1.85% were calculated for DSE 1 and 2 respectively. Gradient and Pearsons correlation coefficients for DSE 1 were estimated as 44.98 deg. and 99.87% respectively,

and for DSE 2 as 45.00 deg. and 99.58%. These metrics indicate very good predictive accuracy for DSE 1 and good accuracy for DSE 2.

Surrogate models for $NO_X$ were also constructed, however, this study conducts a single objective optimization for fuel flow rate. Figure 12 justifies this selection, with an illustration of fuel flow rate versus $NO_X$ rate from every DSE sample point. This indicates the close correlation between $NO_X$ and fuel flow. The variation of $NO_X$ rate to fuel flow rate can primarily be attributed to altitude, as illustrated by the marker shading. This indicates that for a specified operating condition, a fuel flow rate optimal solution will not produce unacceptable $NO_X$ characteristics.
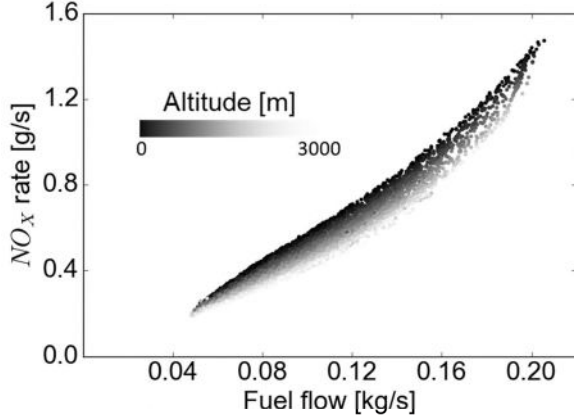


**Figure 12:** Fuel flow versus $NO_X$ rate for all DSE samples

### 3.4 Optimal redundant control design optimization

With surrogate models derived, it was possible to determine the optimal redundant control allocation for any operating condition. Sensitivity analysis for selected points throughout the operational envelope was conducted to determine the population size and the maximum number of generations required to converge the controls to within a $10^{-10}$ change per generation. A population size of 40 individuals and 40 generations was found to be sufficient to attain this criterion.

To assess the impact of operating conditions and the interaction between the three redundant controls, the global optimization method was applied for operating conditions which encompass the rotorcrafts flight envelope. Optimal allocations of the redundant controls and the resulting fuel flow deltas were obtained. The nominal main rotors speed is maintained at 28.7 rad/s, except when the advancing tip Mach number would exceed 0.9, in which case it is reduced. The propeller operates with a fixed gearing ratio to the main rotors, and the fuselage attitude is set at 1 deg., above 40 m/s. Below this flight speed, the fuselage attitude is required to trim the rotorcraft. The effect of independently varying VPS was assessed by conducting two optimizations, the first with the propeller speed coupled to the main rotors speed, and the second allowing it to vary independently.

Figures 13-15 illustrate the optimal allocations for two gross weights, W = 5000 kg and 7000 kg. Figure 13 provides the main rotors speed allocation in the low-speed region, DSE 1, where the propeller is disengaged. Figure 14 presents the case with optimal fuselage attitude and main rotors speed with the propeller engaged but coupled to the main rotors speed, and Fig. 15 presents the case with independently VPS. The main rotors and propeller speeds are presented as a percentage of the nominal speed, while the fuel flow deltas are relative to the nominal case.

Figures 13(a) and (c) indicate the variation in optimal main rotors speed ($\overline{\Omega}_{MR}^{Opt}$) for gross weights of W = 5000 kg and 7000 kg. In the low weight case, it is observed that $\overline{\Omega}_{MR}^{Opt}$ is reduced, with the lower bound of 75% being favorable throughout most of this region. For W = 7000 kg, $\overline{\Omega}_{MR}^{Opt} < 80\%$ occurs only at low altitude near endurance flight speed. The regions where large reductions in $\overline{\Omega}_{MR}^{Opt}$ are optimal decrease with both altitude and reducing flight speed. These trends correspond to the previous discussion, as a result of the increased blade loading at high-altitude, low-speed, or increased weight, reductions in main rotors speed are not as beneficial as insufficient stall-margin is available. The corresponding fuel flow reductions are shown in Figs. 13(b) and (d). $\Delta\dot{m}_f$ of up to -13% are observed at W = 5000 kg, with $\Delta\dot{m}_f$ up to 8% for W = 7000 kg, at low-altitude near endurance flight speeds. The benefits reduce with flight speed and altitude, diminishing rapidly for W = 7000 kg.
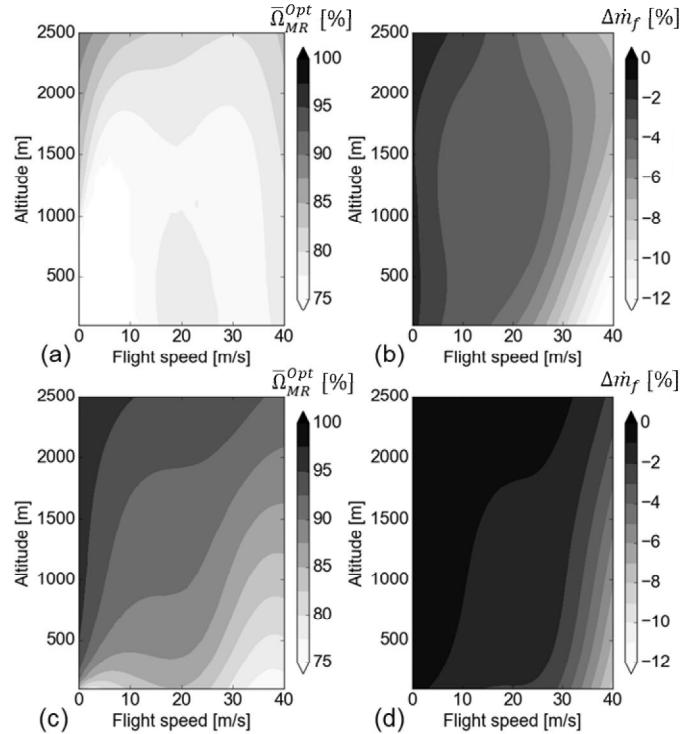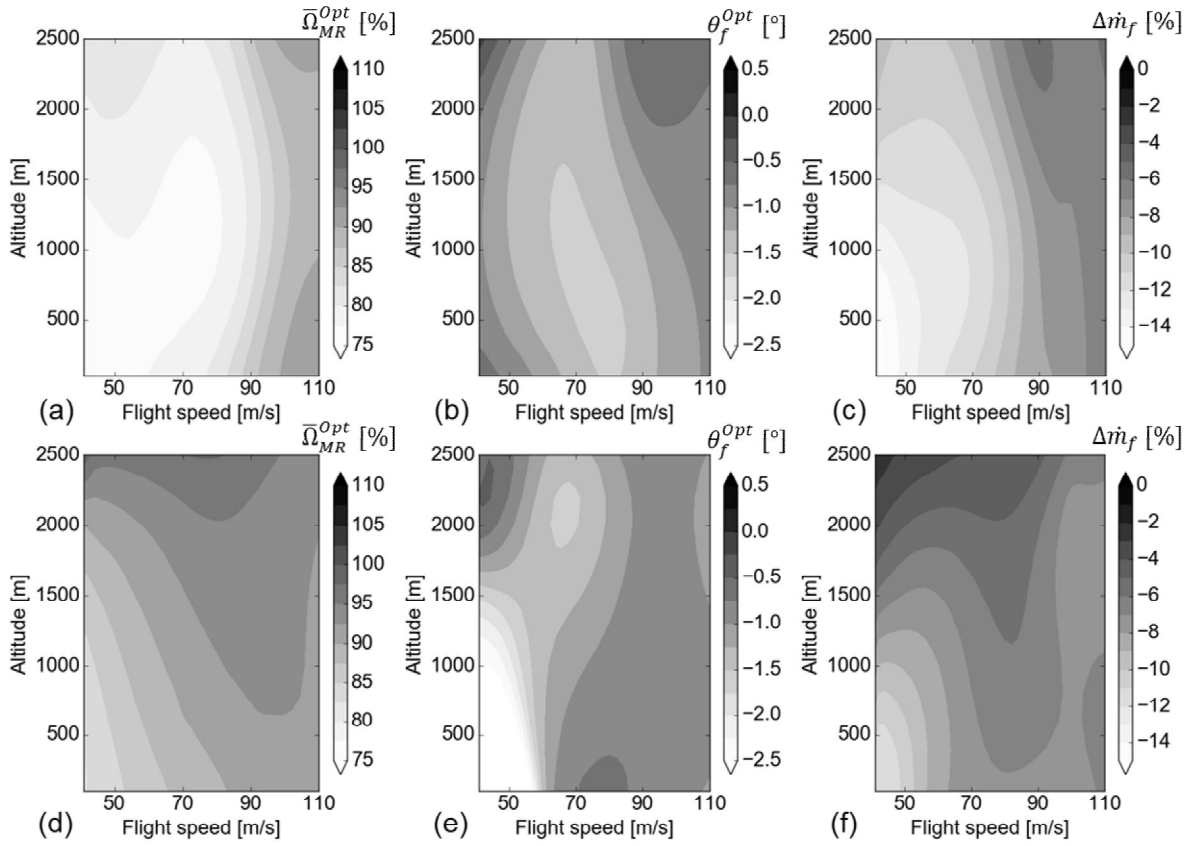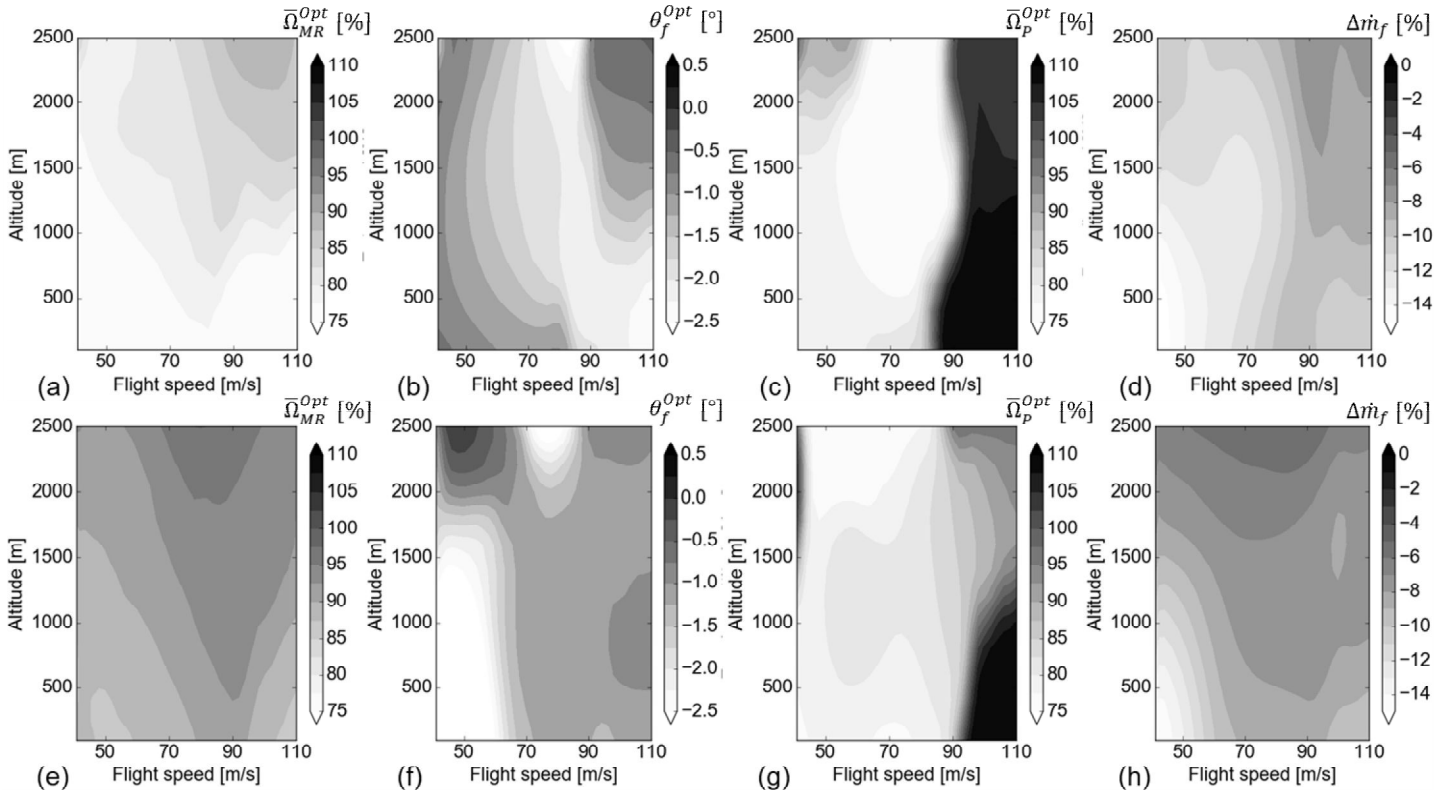


**Figure 13:** Optimal VRS allocation and resultant fuel flow benefit for V = 0-40 m/s, for varied operational conditions: (a, b) W = 5000 kg, and (c, d) W = 7000 kg

Figure 14 presents the V = 40-110 m/s region with optimal fuselage attitude and rotor speed allocation. For W = 5000 kg, $\overline{\Omega}_{MR}^{Opt} < 80\%$ is optimal for the majority of the flight envelope, up to V = 80-95 m/s. Above this speed, an increase in $\overline{\Omega}_{MR}^{Opt}$ is observed. This results from the main rotors-propeller-engine speed trade-off, as in these conditions power demand is high, rising to above MCP at V = 110 m/s. In this state, reducing the engines FPT speed is detrimental to engine performance. Also, the propeller loading is high, and therefore reducing the propellers speed will hinder its aerodynamic performance. These two factors are at odds with the rotor performance as it is desirable to reduce its speed to mitigate transonic drag effects encountered on the advancing blade tips. Similar behavior is observed for W = 7000 kg, Fig. 14(d), albeit with an increase in $\overline{\Omega}_{MR}^{Opt}$ in the V = 40-95 m/s range, particularly with increasing altitude, due to the increasing blade loading.

9

**Figure 14:** Optimal control allocation for VRS and fuselage attitude and resultant fuel flow relative to the nominal case, for varied operational conditions: (a-c) W = 5000 kg, (d-f) W = 7000 kg



**Figure 15:** Optimal control allocation for VRS, fuselage attitude and VPS and resultant fuel flow relative to the nominal case, for varied operational conditions: (a-d) W = 5000 kg, (e-h) W = 7000 kg

The corresponding fuselage attitude allocations are shown in Figs. 14(b) and (e). For the majority of the flight envelope $-1.5 < \theta_f^{Opt} < -0.5$ deg., however, in the W = 7000 kg case at h < 1500 m and V < 60 m/s a region of $\theta_f^{Opt} < -2.5$ deg. is observed. In this condition, it is more efficient to tilt the rotor thrust vector forward, thus offloading the propeller almost entirely so that it generates minimal thrust. For both weights, as flight speed increases the optimal attitude increases. This results from the propeller being able to provide propulsive thrust more efficiently, and the rotor less so at higher speed. The corresponding fuel flow benefits are presented in Figs. 14(c) and (f). For V < 90 m/s the W = 5000 kg demonstrates greater potential fuel savings, resulting from the large reductions in main rotors speed. At higher flight speed the differences between weights reduce as the airframe drag increases, and reduced $\bar{\Omega}_{MR/P}$ is more detrimental to propeller performance than beneficial to main rotors performance.

The impact of independently VPS on optimal redundant control allocations and fuel flow benefits is illustrated in Fig. 15. The optimal main rotors speed trends are shown in Figs. 15(a) and (c), and are similar to those observed in the coupled main rotors-propeller speed case, except for the high-speed conditions. For W = 5000 kg at high altitude and V > 90 m/s a slight reduction in main rotors-speed relative to the fixed main rotors-propeller speed is seen. At low altitude, this is more pronounced, with $\bar{\Omega}_{MR}^{Opt}$ reducing to 75% for V > 80 m/s and h < 1000 m. This results from removing the propeller from the main rotors-engine speed trade-off. In high-speed flight, a high propeller speed is demanded due to high thrust requirement, but a low main rotors speed may mitigate transonic effects and reduce profile power. In the W = 7000 kg case, there is a smaller change except for V > 90 m/s and h < 1000 m, where $\bar{\Omega}_{MR}^{Opt}$ reduced from around 90% to less than 85%. Higher main rotors speed is maintained relative to W = 5000 kg due to the larger W and hence higher rotor blade loading.

For W = 5000 kg, the trends of optimal fuselage attitude are similar to Fig. 14. However, there is a region where $\theta_f^{Opt} < -2$ deg., between V = 80-90 m/s. For h < 1000 m this is extended to the maximum flight speed. For W = 7000 kg this region does not occur, and similar trends to the fixed main rotors-propeller speed are shown, with a slight decrease in $\theta_f^{Opt}$ observed throughout most of the flight envelope. The region of low $\theta_f^{Opt}$ for V < 60 m/s is slightly extended in both speed and altitude, with a second region of $\theta_f^{Opt} < -2.5$ deg. occurring at high altitude from V = 70-80 m/s.

The optimal propeller speed allocation for W = 5000 and W = 7000 kg are shown in Figs. 15(c) and (g). Both cases show that $\bar{\Omega}_P^{Opt} < 80\%$ is optimal below V = 80-95 m/s. A switch in propeller speed to $\bar{\Omega}_P^{Opt} > 100\%$ is then observed above V = 85-95 m/s in the W = 5000 kg case, and above V = 90-100 m/s at low altitude in the W = 7000 kg case. For W = 7000 kg, h > 1000 m, $\bar{\Omega}_P^{Opt}$ increases more gradually with flight speed. This switch in operating conditions between a low and high propeller speed result from two local optima. The first condition is a low propeller loading and hence low optimal propeller speed, with a larger negative attitude and thus lower net rotor drag. The second is a high propeller thrust condition, with higher rotor drag. The maximum benefit relative to the fixed gearing ratio case occurs at low h, low W, and high V, with $\Delta \dot{m}_f$ of -4.8%. This

corresponds to high propeller but low rotor loading, therefore high $\bar{\Omega}_P^{Opt}$ but low $\bar{\Omega}_{MR}^{Opt}$ is optimal.

In this section, the optimal allocation of the redundant controls has been presented for the generic coaxial rotorcraft. The potential benefits of utilizing VPS has been separated from VRS and fuselage attitude, which also illustrated the impact the propeller has on the optimal VRS trade-off.

### 3.5 Synthesis of optimal control allocation

The understanding garnered in the previous section provides insight into allocating the redundant controls during actual operations. It is important to appreciate the key trends and governing principles from this, which dictate the optimal redundant controls. In the low-speed region, Fig. 13, the level of main rotor loading is the key element. $\bar{\Omega}_{MR}^{Opt}$ increases with both gross weight and altitude. As flight speed increases, $\bar{\Omega}_{MR}^{Opt}$ decreases as induced power reduces and profile power becomes critical. As a result, $\bar{\Omega}_{MR}^{Opt}$ increases from 75% at low gross weight and altitude, to between 95-102% at high gross weight and altitude.

Figure 14 illustrates V = 40-110 m/s with $\bar{\Omega}_P = \bar{\Omega}_{MR}$. $\bar{\Omega}_{MR}^{Opt} = 75\%$ at low gross weight, low altitude, and V = 40 m/s, increasing with each of W and h up to $\bar{\Omega}_{MR}^{Opt} = 100\%$. The associated $\Delta \dot{m}_f$ also tends to decrease as $\bar{\Omega}_{MR}^{Opt}$ increases. As for lower flight speeds, higher gross weight and altitude tend to increase the main rotors blade loading, and hence $\bar{\Omega}_{MR}^{Opt}$. Flight speed tends to raise propeller blade loading, hence in the non-VPS case, $\bar{\Omega}_{MR}^{Opt}$ also increases. Also, at higher flight speeds, the power required increases, which leads to a larger detriment in engine performance when $\bar{\Omega}_{MR}$ is reduced. This results in maximum benefits of $\Delta \dot{m}_f = -15.35\%$, at V = 40 m/s, h = 0 m, W = 5000 kg, with $\bar{\Omega}_{MR}^{Opt} = 75.9\%$ and $\theta_f^{Opt} = -0.6$ deg.

In the VPS case, Fig. 15, the optimal schedules show broadly the same behavior. The main differences occur at high flight speeds and lower gross weight, where a reduction in $\bar{\Omega}_{MR}$ is enabled by VPS. The maximum benefit this provides is at h < 500, V = 110 m/s, W = 5000 kg, with fuel flow reduced by 4.8% relative to the $\bar{\Omega}_P = \bar{\Omega}_{MR}$ case.

It is apparent that all three redundant controls considered may provide significant benefits in various regions of the operational envelope. $\theta_f$ provides a reduction relative to nominal throughout the entire envelope, however, $\theta_f^{Opt}$ varies only slightly outside of the low flight speed, low altitude region, where it contributes significantly to $\Delta \dot{m}_f$. $\bar{\Omega}_{MR}$ is most beneficial for low-loading cases, and its impact is limited at high flight speed due predominantly to the engine and propeller performance implications. VPS relieves this limitation, providing improvements at low flight speed, where the propeller is very lightly loaded, and high-speed when highly loaded.

### 3.6 Mission level assessment

The impact of optimal redundant control allocation at mission level rather than idealized trim points provides a more realistic assessment of the benefits that these technologies may provide. Three missions were defined which are considered representative of expected civilian operations of future rotorcraft. An emergency medical service (EMS), SAR, and PAT mission were used to assess the wide variety of conditions which rotorcraft operate in. Figure 17 illustrates the altitude and flight speed profiles for each.

11

In the EMS mission, Fig. 17(a), the rotorcraft takes-off from its base and flies to the area of a hypothetical incident, where it lands and collects a single casualty. The casualty is transported to a local hospital before the rotorcraft returns to its base. The rotorcraft cruises at h = 1500 m, V = 105 m/s in the first two, time critical legs. Fig. 17(b) illustrates the SAR mission. The rotorcraft takes off from its base heliport and flies to a search area, where it reduces its altitude and flies a search pattern at h = 90 m and V = 50 m/s until finding the hypothetical incident from which two casualties are recovered. They are flown to a local hospital, from which the rotorcraft returns to its base. The banked turns required to conduct a search pattern are not accounted for, with the rotorcraft considered to fly level and straight for the duration of the search segment. For the PAT mission shown in Fig. 17(c), the rotorcraft transfers 12 passengers on a single legged journey at h = 2500 m and V = 90 m/s.

Extension of the assessment to mission level also required allocation of the redundant controls in climbing and descending flight. The climb and descent conditions are maintained at a horizontal flight speed of 80 m/s, with a climb or descent rate of ±8 m/s. For these two conditions, parametric sweeps were conducted to select the redundant controls. $\theta_f$ in climb and descent is used for every case, including the nominal. In climb, $\bar{\Omega}_P$ and $\bar{\Omega}_{MR}$ are kept at nominal, while in descent $\bar{\Omega}_P = \bar{\Omega}_{MR} = 90\%$, providing further benefits when applied.

The total mission fuel, $CO_2$, and $NO_X$ deltas relative to the nominal are shown in Fig. 16. The nominal case represents the state of the art, utilizing a fixed gearing ratio between the main rotors and propeller, with main rotors speed reduced at high-speed to maintain tip Mach number less than 0.9 [40]. Best practice suggested in the literature was applied for the fuselage attitude when redundant, $\theta_f = 1$ deg. [4,5]. To isolate the effects of the three redundant controls, each mission was run three times, with an increasingly complex control system: (a) optimal fuselage attitude, nominal main rotors speed, and a fixed-gearing ratio propeller, (b) optimal fuselage attitude, optimal main rotors speed, and a fixed gearing ratio propeller, and (c) optimal fuselage attitude, optimal main rotors speed, and optimally independently variable propeller speed. The fuel and $NO_X$ rates throughout the missions are shown in Fig. 18 for the nominal and case (c).
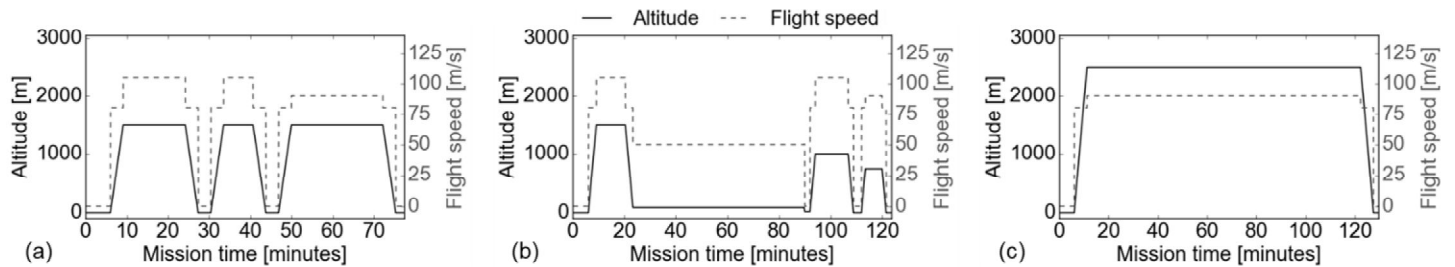
For the EMS mission, fuselage attitude optimization provides a 1.81% fuel burn and 2.07% $NO_X$ reduction. Optimal VRS allocation increases the level of fuel burn reduction to 4.19%. This is due to a reduction in main rotors speed to $\bar{\Omega}_{MR} = 85\text{-}89\%$ during cruise, which is viable due to the rotorcraft weight being low, W = 5500 – 6000 kg, throughout the mission. Also, applying $\bar{\Omega}_{MR} = 81\%$ in hover provides further benefits. The application of VPS to this mission has provided a further reduction of 0.52% in fuel burn, resulting from an increase in $\bar{\Omega}_P$ and slight reduction in $\bar{\Omega}_{MR}$ from the coupled case in cruise.



**Figure 16:** Impact of optimum redundant control allocation on mission fuel burn, $CO_2$, and $NO_X$ emissions

The greatest improvement was observed in the SAR mission. A 3.70% fuel burn reduction is provided by fuselage attitude optimization, rising to 6.15% with VRS. This results principally from applying $\bar{\Omega}_{MR} = 80\%$ in search, which provides an 11% fuel flow reduction. Allowing the propeller to reach an independently optimum speed gives a further 0.78% fuel burn reduction, with the propeller speed reduced to $\bar{\Omega}_P = 75\%$ in search. In high-speed cruise, an increase in propeller speed is applied alongside a decrease in main rotor speed to provide further engine performance improvement. Fig. 18(b) demonstrates this, with the largest relative reduction in the search segment.



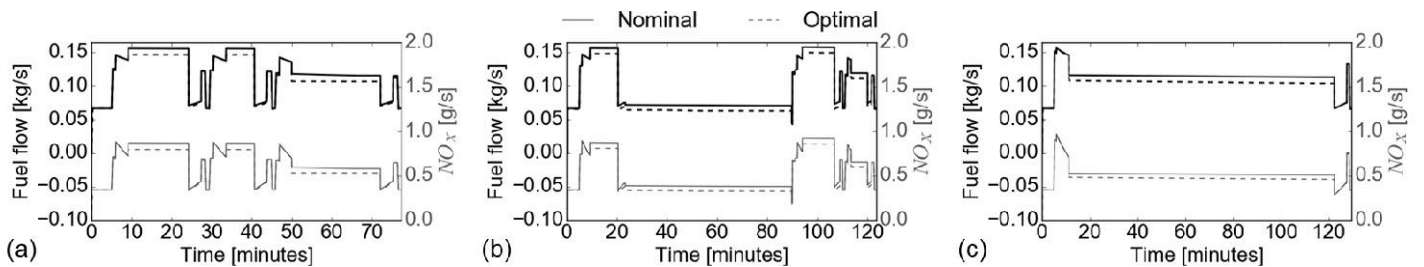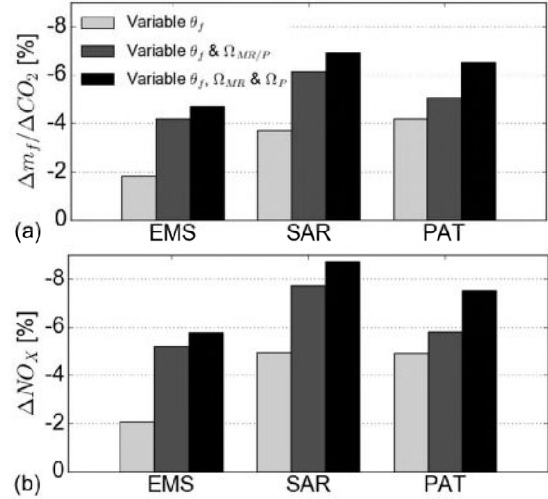**Figure 17:** Mission altitude and flight speed profiles: (a) EMS, (b) SAR, and (c) PAT



**Figure 18:** Comparison of mission fuel flow and $NO_X$ rates for nominal and optimized controls: (a) EMS, (b) SAR, and (c) PAT

For the PAT mission, a 4.2% fuel flow reduction is provided solely from fuselage attitude optimization. With the addition of optimal main rotor and propeller speed, this rises to 5.06%. For this mission, the benefits from VRS are low due to the high altitude cruise at a relatively high gross weight. Here, VPS provides notable improvements, with a further 1.47% fuel burn reduction with $\overline{\Omega}_P = 104\text{-}106\%$ and $\overline{\Omega}_{MR} = 94\text{-}97\%$ during cruise. This level of fuel reduction is attained due to the large proportion of the mission spent in steady cruise relative to the other cases. Fig. 18(c) shows that the benefit relative to the nominal case increases with flight time, as the rotorcrafts weight decreases, and hence a lower main rotors speed is applied.

It has been demonstrated that the engine performance enhancement from optimal redundant control allocation of a coaxial compound rotorcraft depends strongly on the mission type. Optimally allocating the fuselage attitude provides gains for all scenarios. VRS is particularly beneficial when the rotorcraft is lightly loaded or flying near endurance flight speed. VPS benefits are restricted to cases where the optimal main rotors-engine speed is far from the propeller optimum.

## 4 CONCLUSION

This study investigated the potential engine performance benefits for a coaxial compound rotorcraft from optimal redundant control allocation. An integrated simulation framework for rotorcraft flight performance, engine performance and combustor pollutant emissions was developed and validated. A generic coaxial compound rotorcraft configuration was developed to enable this assessment. The impact of fuselage attitude, VRS, and VPS on engine performance were analyzed. Allocation of the optimal redundant controls for any operating condition was enabled by the deployment of a DSE, surrogate modeling and global optimization method, enabling extension of the assessments to mission level.

Determining the optimal main rotors speed was shown to require a multi-disciplinary approach, which includes the main rotors, engine, and propeller implications to be assessed together. For low gross weight, altitude, or near endurance flight speed, a reduced main rotors speed can provide aerodynamic and engine thermodynamic improvements resulting in a fuel flow reduction of up to 10.22%. Decoupling the propeller speed from the main rotors speed was shown to provide a further reduction in some high and low-speed conditions of up to 4.80%. Mission level assessment demonstrated fuel burn reductions for optimal fuselage attitude allocation and VRS ranging from 4.19% to 6.15%, rising to 6.93% when VPS is enabled. The corresponding $NO_X$ reductions were consistently higher, ranging from 5.21% to 8.74%. Although VPS provided some performance improvements, an accurate estimate of weight for such a system is required to determine conclusively if a benefit is attainable.

This work has provided new insight into the impact of optimal redundant control allocation toward engine performance enhancement of a compound rotorcraft. Best practices for optimal redundant control allocation have been presented, demonstrating significant reductions in fuel burn and $NO_X$ emission of up to 6.93% and 8.74% respectively.

## ACKNOWLEDGEMENTS

## REFERENCES

[1] Blackwell, R., and Millott, T., "Dynamics Design Characteristics of the Sikorsky X2 Technology™ Demonstrator Aircraft," *64th Annual Forum of the American Helicopter Society*, (2008).

[2] Walsh, D., Weiner, S., Arifian, K., Lawrence, T., Wilson, M., Millott, T., and Blackwell, R., "High Airspeed Testing of the Sikorsky X2 Technology™ Demonstrator," *67th Annual Forum of the American Helicopter Society*, (2011).

[3] Colucci, F., "Scaling Up Success," Vertiflite, Vol.62 No.1, (2016).

[4] Jacobellis, G., Gandhi, F., and Floros, M., "Using Control Redundancy for Power and Vibration Reduction on a Coaxial Rotor Helicopter at High Speeds," Journal of the American Helicopter Society, Vol.64 No.3, (2019), pp. 1–15, DOI https://doi.org/10.4050/JAHS.64.032008.

[5] Herrmann, T. A., Celi, R., and Baeder, J. D., "Multidisciplinary Trim Analysis of a Coaxial-Pusher Rotorcraft Configuration," *74th Annual Forum of the American Helicopter Society*, (2018).

[6] Herrmann, T. A., Celi, R., and Baeder, J. D., "Multidisciplinary, Multiobjective Trim Optimization for a Coaxial-Pusher Rotorcraft Configuration," *Vertical Flight Society 75th Annual Forum & Technology Display*, (2019).

[7] Padfield, G. D., *Helicopter Flight Dynamics - the Theory and Application of Flying Qualities and Simulation Modelling*, John Wiley & Sons, Chichester, UK, (2007).

[8] Reddinger, J.-P., and Gandhi, F., "Physics-Based Trim Optimization of an Articulated Slowed-Rotor Compound Helicopter in High-Speed Flight," Journal of Aircraft, Vol.52 No.6, (2015), pp. 1756–1766, DOI 10.2514/1.C032939.

[9] Reddinger, J.-P., and Gandhi, F., "Neural Network and Machine Learning Allocation of Redundant Controls for Power Optimization on a Compound Helicopter," 73rd Annual Forum of the American Helicopter Society, (2017), pp. 1507–1519.

[10] Reddinger, J.-P., Gandhi, F., and Kang, H., "Using Control Redundancy for Power and Vibration Reduction on a Compound Helicopter at High Speeds," Journal of the American Helicopter Society, Vol.63 No.3, (2018), pp. 032009-1-032009–13, DOI 10.4050/JAHS.63.032009.

[11] Misté, G. A., and Benini, E., "Performance of a Turboshaft Engine for Helicopter Applications Operating at Variable Shaft Speed," ASME Gas Turbine India Conference, (2012), pp. 701–715, DOI 10.1115/GTINDIA2012-9505.

[12] Misté, G. A., Benini, E., Garavello, A., and Gonzalez-Alcoy, M., "A Methodology for Determining the Optimal Rotational Speed of a Variable RPM Main Rotor/Turboshaft Engine System," Journal of the American Helicopter Society, Vol.60 No.3, (2015), pp. 1–11, DOI 10.4050/jahs.60.032009.

[13] Misté, G. A., and Benini, E., "Variable-Speed Rotor Helicopters: Performance Comparison Between Continuously Variable and Fixed-Ratio Transmissions," Journal of Aircraft, Vol.53 No.5, (2016), pp. 1189–1200, DOI 10.2514/1.c032744.

[14] Goulos, I., and Bonesso, M., "Variable Rotor Speed and Active Blade Twist for Civil Rotorcraft: Optimum Scheduling, Mission Analysis, and Environmental Impact," Aerospace Science and Technology, Vol.88 , (2019), pp. 444–456, DOI 10.1016/j.ast.2019.03.040.

[15] Han, D., and Barakos, G. N., "Variable-Speed Tail Rotors for Helicopters with Variable-Speed Main Rotors," Aeronautical Journal, Vol.121 No.1238, (2017), pp. 433–448, DOI

10.1017/aer.2017.4.

[16] Garcia, T. A., "MULTI - SPEED GEARBOX FOR TAIL ROTOR OF A COMPOUND HELICOPTER," No. US 2018 / 0215463 A1 (2018).

[17] MacMillan, W. L., "Development of a Modular-Type Computer Program for the Calculation of Gas Turbine off-Design Performance," Ph.D. Thesis, Cranfield University, (1974).

[18] Celis, C., "Evaluation and Optimisation of Environmentally Friendly Aircraft Propulsion Systems," Ph.D. Thesis, Cranfield University, (2010).

[19] van der Wall, B. G., "The Effect of HHC on the Vortex Convection in the Wake of a Helicopter Rotor," Aerospace Science and Technology, Vol.4 No.5, (2000), pp. 321–336, DOI 10.1016/S1270-9638(00)00141-3.

[20] Yana, J., and Rand, O., "Performance Analysis of a Coaxial Rotor System in Hover: Three Points of View," 28th International Congress of the Aeronautical Sciences, (2012).

[21] Enconniere, J., Ortiz-Carretero, J., and Pachidis, V., "Mission Performance Analysis of a Conceptual Coaxial Rotorcraft for Air Taxi Applications," Aerospace Science and Technology, Vol.69 , (2017), pp. 1–14, DOI 10.1016/j.ast.2017.06.015.

[22] Hersey, S., Sridharan, A., and Celi, R., "Multiobjective Performance Optimization of a Coaxial Compound Rotorcraft Configuration," Journal of Aircraft, Vol.54 No.4, (2017), pp. 1498–1507, DOI 10.2514/1.C033999.

[23] Leishman, J. G., *Principles of Helicopter Aerodynamics*, Cambridge University Press, (2006).

[24] Harendra, P. B., Joglekar, M. J., Gaffey, T. M., and Marr, R. L., *V/STOL Tilt Rotor Study - Volume V: A Mathematical Model For Real Time Flight Simulation of the Bell Model 301 Tilt Rotor Research Aircraft*, Bell Helicopter Company Report No. 301-099-001, (1973).

[25] Harris, D. F., *Intoduction to Autogyros, Helicopters and Other V/STOL Aircraft: Volume II Helicopters*, NASA/SP–2012-215959, (2012).

[26] Yeo, H., "Design and Aeromechanics Investigation of Compound Helicopters," Aerospace Science and Technology, Vol.88 , (2019), pp. 158–173, DOI 10.1016/j.ast.2019.03.010.

[27] Johnson, W., *NDARC NASA Design and Analysis of Rotorcraft: Theory*, NASA/TP–2015-218751, (2018).

[28] Yeo, H., and Johnson, W., "Investigation of Maximum Blade Loading Capability of Lift-Offset Rotors," Journal of the American Helicopter Society, Vol.59 No.1, (2013), pp. 1–12, DOI 10.4050/jahs.59.012005.

[29] Johnson, W., *Influence of Lift Offset on Rotorcraft Performance*, Nasa/Tp-2009-215404, (2009).

[30] Goulos, I., Hempert, F., Sethi, V., Pachidis, V., D'Ippolito, R., and D'Auria, M., "Rotorcraft Engine Cycle Optimization at Mission Level," Journal of Engineering for Gas Turbines and Power, Vol.135 No.9, (2013), DOI 10.1115/1.4024870.

[31] Ortiz-Carretero, J., Castillo Pardo, A., Goulos, I., and Pachidis, V., "Impact of Adverse Environmental Conditions on Rotorcraft Operational Performance and Pollutant Emissions," Journal of Engineering for Gas Turbines and Power, Vol.140 No.2, (2017), DOI 10.1115/1.4037751.

[32] Celis, C., Moss, B., and Pilidis, P., "Emissions Modelling for the Optimisation of Greener Aircraft Operations," *Proceedings of the ASME Turbo Expo*, (2009), pp. 167–178, DOI 10.1115/GT2009-59211.

[33] Goulos, I., Ali, F., Tzanidakis, K., Pachidis, V., and D'Ippolito, R., "A Multidisciplinary Approach for the Comprehensive Assessment of Integrated Rotorcraft–Powerplant Systems at Mission Level," Journal of Engineering for Gas Turbines and Power, Vol.137 No.1, (2014), DOI 10.1115/1.4028181.

[34] Goulos, I., Giannakakis, P., Pachidis, V., and Pilidis, P., "Mission Performance Simulation of Integrated Helicopter–Engine Systems Using an Aeroelastic Rotor Model," Journal of Engineering for Gas Turbines and Power, Vol.135 No.9, (2013), DOI 10.1115/1.4024869.

[35] Olsson, A., Sandberg, G., and Dahlblom, O., "On Latin Hypercube Sampling for Structural Reliability Analysis," Structural Safety, Vol.25 No.1, (2003), pp. 47–68.

[36] Pedregosa, F. and Varoquaux, G. and Gramfort, A. and Michel, V., and Thirion, B. and Grisel, O. and Blondel, M. and Prettenhofer, P., and Weiss, R. and Dubourg, V. and Vanderplas, J. and Passos, A. and, and Cournapeau, D. and Brucher, M. and Perrot, M. and Duchesnay, E., "Scikit-Learn: Machine Learning in Python," Journal of Machine Learning Research, Vol.12 , (2011), pp. 2825--2830, doi.org/10.1016/S0167-4730(02)00039-5.

[37] Arlot, S., "A Survey of Cross-Validation Procedures for Model Selection," Statistics Surveys, Vol.4 , (2010), pp. 40–79, DOI 10.1214/09-SS054.

[38] Deb, K., Pratap, A., Agarwal, S., and Meyarivan, T., "A Fast and Elitist Multiobjective Genetic Algorithm: NSGA-II," *EEE Transactions on Evolutionary Computation*, (2002), pp. 182–197, 10.1109/4235.996017.

[39] "Fast Rotorcraft IADP" [Online]. Available: https://www.cleansky.eu/fast-rotorcraft-iadp. [Accessed: 02-Nov-2019].

[40] Bagai, A., "Aerodynamic Design of the X2 Technology Demonstrator[TM] Main Rotor Blade," *64th Annual Forum of the American Helicopter Society*, (2008).

[41] Passe, B. J., Sridharan, A., and Baeder, J. D., "Computational Investigation of Coaxial Rotor Interactional Aerodynamics in Steady Forward Flight," *33rd AIAA Applied Aerodynamics Conference*, (2015), DOI 10.2514/6.2015-2883.

[42] "S-97 Raider Demonstrator," (2019) [Online]. Available: www.lockheedmartin.co.uk/en-us/products/s-97-raider-helicopter.html. [Accessed: 10-Nov-2019].

[43] Yuan, Y., Thomson, D., and Chen, R., "Propeller Control Strategy for Coaxial Compound Helicopters," Proceedings of the Institution of Mechanical Engineers, Part G: Journal of Aerospace Engineering, Vol.233 No.10, (2018), pp. 3775–3789, DOI 10.1177/0954410018806796.

[44] Johnson, W., Moodie, A. M., and Yeo, H., "Design and Performance of Lift-Offset Rotorcraft for Short-Haul Missions," *American Helicopter Society Future Vertical Lift Aircraft Design Conference*, (2012).

[45] Evans, A. J., and Liner, G., *A Wind-Tunnel Investigation of the Aerodynamic Characteristics of a Full-Scale Sweptback Propeller and Two Related Straight Propellers*, NACA RM L50J05, (1951).

[46] Daley, B. N., and Lord, D. R., *Aerodynamic Characteristics of Several 6% Thick Airfoil at Angle of Attack from $0^0$ to $20^0$ at High Subsonic Speed*, NACA TN 3424, (1955).

[47] Gur, O., and Rosen, A., "Comparison between Blade-Element Models of Propellers," Aeronautical Journal, Vol.112 No.1138, (2008), pp. 689–704, DOI 10.1017/S0001924000002669.

[48] Ballin, M. G., *A High Fidelity Real-Time Simulation of a Small Turboshaft Engine*, NASA TM 100991, (1988).

[49] Garavello, A., and Benini, E., "Preliminary Study on a Wide-Speed-Range Helicopter Rotor/Turboshaft System," Journal of Aircraft, Vol.49 No.4, (2012), pp. 1032–1038, DOI 10.2514/1.C031526.

[50] Johnson, W., Elmore, J. F., Keen, E. B., Gallaher, A. T., and Nunez, G. F., "Coaxial Compound Helicopter for Compound Urban Operations," *American Helicopter Society Technical Meeting on Aeromechanics Design for Vertical Lift*, (2016).

2021-01-11

# Optimal control of a compound rotorcraft for engine performance enhancement

## Scullion, Calum

ASME

Scullion C, Vouros S, Goulos I, et al., (2020) Optimal control of a compound rotorcraft for engine performance enhancement. In: ASME Turbo Expo 2020, 21-25 September 2020, London, Virtual Event. Paper number GT2020-16280

https://doi.org/10.1115/GT2020-16280